INSTITUTE OF PHYSICS PUBLISHING and INTERNATIONAL ATOMIC ENERGY AGENCY NUCLEAR FUSION

Nucl. Fusion **46** (2006) 162–170 doi:10.1088/0029-5515/46/1/018

Numerical study of the formation, ion spin-up and nonlinear stability properties of field-reversed configurations

E.V. Belova[1], R.C. Davidson[1], H. Ji[1], M. Yamada[1], C.D. Cothran[2], M.R. Brown[2] and M.J. Schaffer[3]

[1] Princeton Plasma Physics Laboratory, Princeton, NJ, USA
[2] Swarthmore College, Swarthmore, PA, USA
[3] General Atomics, San Diego, CA, USA

E-mail: ebelova@pppl.gov

Received 11 May 2005, accepted for publication 17 November 2005
Published 22 December 2005
Online at stacks.iop.org/NF/46/162

Abstract

Results of three-dimensional (3D) numerical simulations of field-reversed configurations (FRCs) are presented. The emphasis of this work is on the nonlinear evolution of magnetohydrodynamic (MHD) instabilities in kinetic FRCs and the new FRC formation method by counter-helicity spheromak merging. Kinetic simulations show nonlinear saturation of the $n = 1$ tilt mode, where n is the toroidal mode number. The $n = 2$ and $n = 3$ rotational modes are observed to grow during the nonlinear phase of the tilt instability due to the ion spin-up in the toroidal direction. The ion toroidal spin-up is shown to be related to the resistive decay of the internal flux and the resulting loss of particle confinement. Three-dimensional MHD simulations of counter-helicity spheromak merging and FRC formation show good qualitative agreement with the results from the SSX–FRC experiment. The simulations show the formation of an FRC in about 20–30 Alfvén times for typical experimental parameters. The growth rate of the $n = 1$ tilt mode is shown to be significantly reduced compared with the MHD growth rate due to the large plasma viscosity and field-line-tying effects.

PACS numbers: 52.55.Lf, 52.65.Kj, 52.65.Rr, 52.35.Vd

(Some figures in this article are in colour only in the electronic version)

1. Introduction

The field-reversed configuration (FRC) is a compact toroid with little or no toroidal field. It offers a unique fusion reactor potential because of its compact and simple geometry, translation properties and high plasma beta [1]. At present, the most important issues are FRC stability with respect to low-n (toroidal mode number) magnetohydrodynamic (MHD) modes and the development of new FRC formation and current-drive methods.

The traditional theta-pinch formation method usually produces highly kinetic FRCs with relatively low flux, small S^* (the FRC kinetic parameter S^* is the ratio of the separatrix radius to the ion skin depth) and large elongation E. A theoretical understanding of the observed FRC stability properties has proved to be elusive due to the complicated interplay of several non-ideal MHD effects [2–4], including finite-Larmor-radius (FLR) effects, the Hall term and plasma flow effects. Advanced numerical simulations are required to describe the self-consistent stability properties of kinetic FRCs [3, 5, 6]. The results of a set of such simulations are presented in this paper.

A slow FRC formation technique, based on counter-helicity spheromak merging, has demonstrated the advantage of this approach compared with traditional theta-pinch formation methods [7]. The counter-helicity spheromak merging method allows the formation of the configuration with large-S^*, thus permitting experimental studies of large-S^* FRC stability properties. The SSX–FRC experiment [8] is designed to study FRC formation by the counter-helicity spheromak merging method and to examine the general issue of FRC stability properties at large S^*. Three-dimensional (3D) MHD simulations have been performed in support of the SSX–FRC experiment and show good agreement with the experimental results.

2. Study of FRC nonlinear stability properties

Numerical studies of the nonlinear evolution of MHD instabilities in kinetic, prolate FRCs (theta-pinch-formed FRCs) have been performed using the 3D nonlinear hybrid and MHD simulation code HYM [5]. The stability properties of MHD modes with toroidal mode numbers $n \geqslant 1$ have been investigated, including finite-ion-Larmor radius (FLR) and rotational effects. It has been demonstrated that due to the strong FLR stabilization of the higher-n modes, the $n = 1$ tilt mode is the most unstable mode for nearly all experimentally-relevant non-rotating FRC equilibria [3]. An empirical FLR scaling of the tilt mode linear growth rate has been obtained: $\gamma = CV_A/R_sE\exp(-3E\rho_i/R_s)$, where $\gamma_{mhd} = CV_A/R_sE$ is the MHD growth rate, R_s is the separatrix radius, E is the separatrix elongation, ρ_i is the ion thermal Larmor radius and $C \approx 2$ is a constant.

Nonlinear kinetic simulations performed for a set of FRC equilibria with $E = 4$–6 and $S^* = 10$–80 show that the $n = 1$ tilt mode saturates nonlinearly without destroying the configuration, provided the FRC kinetic parameter is sufficiently small, $S^* \lesssim 20$. In addition to the saturation of the tilt mode, nonlinear hybrid simulations show that the ions spin up toroidally in the ion diamagnetic direction, and the $n = 2$ mode grows in the nonlinear phase of the simulation. Initial conditions for the simulations have been set at $t = 0$ so that all of the equilibrium toroidal current is carried by the electrons, and the ions have a non-rotating Maxwellian distribution. These initial conditions are consistent with experimental observations just after FRC formation. However, as the simulation proceeds, the ions gradually begin to rotate, and near the end of the simulation run the ion toroidal flow velocity becomes comparable to the ion diamagnetic velocity.

Therefore, the saturation of the tilt instability occurs in the presence of a significant ion toroidal rotation, and it is accompanied by the growth of the $n = 2$ rotational mode, which is often seen in experiments [1]. The saturation of the $n = 1$ tilt mode and the growth of the $n = 2$ rotational mode can be seen in figure 4 of [3], where the results of nonlinear hybrid simulations are shown for a configuration with $E = 6.25$ and $S^* \approx 20$ (for comparison, the parameters for typical theta-pinch FRC experiments [1] are $E = 5$–8 and $S^* \lesssim 20$). In the nonlinear phase, the ion rotation rate is comparable to the linear growth rate of the tilt mode. Therefore, the ion toroidal spin-up, in addition to driving the rotational instability, is likely to contribute significantly to the saturation of the tilt instability.

2.1. Ion spin-up

A set of two-dimentional (2D) (axisymmetric) nonlinear hybrid simulations has been performed using the HYM code in order to study the resistive evolution of the kinetic FRC and investigate the mechanism of the ion toroidal spin-up. The initial ion distribution function is taken to be $f = f(\varepsilon) = A\exp(-\varepsilon/T_0)$, where $\varepsilon = m_i v^2/2 + e\phi$ is the ion energy, T_0 is the (uniform) ion temperature and ϕ is the electrostatic potential. Since the ion pressure is scalar, a kinetic equilibrium for the hybrid runs has been constructed similar to the ideal MHD equilibrium, i.e. by solving the Grad–Shafranov equation for a chosen pressure profile. The cold-fluid description is used for the electrons, and quasi-neutrality is assumed. The numerical simulations have been performed for an FRC with $E = 4$, $S^* = 20$, and an elliptical separatrix shape. The value of the normalized resistivity at the field null is $\eta_o = 1/S = 10^{-4}$, where $S = V_A R_c/\eta$ is the Lindquist number, and a resistivity profile has been used with η inversely proportional to the plasma density. Periodic boundary conditions have been used in the axial direction, and perfectly conducting boundary conditions have been used at the radial wall.

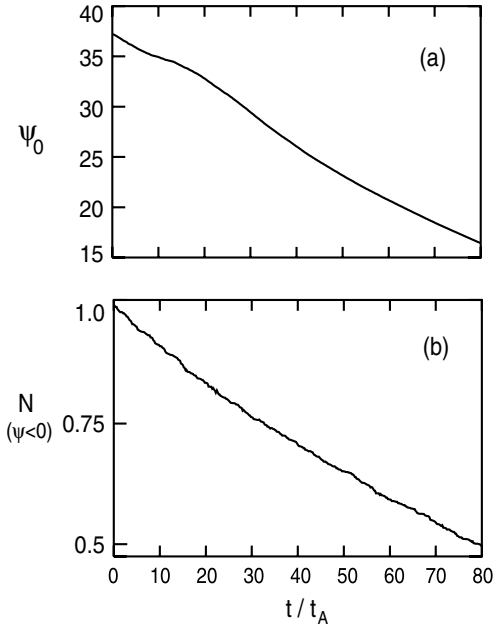

Figure 1. Time evolution of (*a*) the normalized value of trapped poloidal flux and (*b*) the normalized number of ions inside the separatrix obtained from 2D hybrid simulations with $S^* = 20$ and $E = 4$.

The simulations show that there is a significant particle loss associated with the resistive decay of the poloidal flux. Namely, the magnetic field decay results in a slow change in the particle trajectories, so that some of the initially weakly-confined ion trajectories eventually change into open-field-line trajectories. Particles, which change their orbit from closed-field-line into open-field-line orbit at some point during the simulations, are considered 'lost particles' in this paper. Figure 1 shows the time evolution of the trapped poloidal flux $\psi_0(t)$ and the number of ions inside the separatrix region $\psi < 0$. It can be seen that the decay of the poloidal flux results in the loss of a significant fraction of the particles at $t \gtrsim 50t_A$. Here, the Alfvén time is defined as $t_A = R_c/V_A$, where R_c is the radius of the flux conserving shell and V_A is the characteristic Alfvén velocity defined in terms of external magnetic field magnitude and the peak plasma density. Analysis of the particle phase-space shows that the particles with initial values of p_ϕ such that $0 < p_\phi \lesssim \Delta\psi$ are lost from the closed-field-line region when the absolute value of the trapped poloidal flux ψ_0 is reduced by $\Delta\psi$. Here $p_\phi = m_i/eRv_\phi - \psi$ is the canonical toroidal angular momentum of the ion, and the signs are chosen such that condition $p_\phi > 0$ corresponds to an approximate confinement condition. It is also found that most of the lost

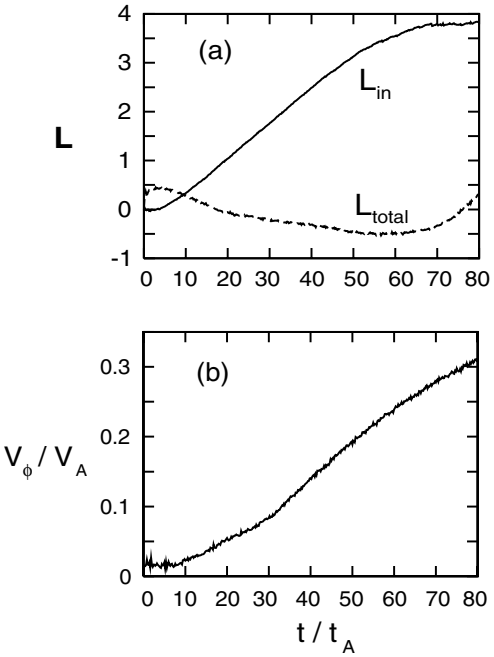

Figure 2. (*a*) Time evolution of the normalized angular momentum of all ions and the ions inside the separatrix and (*b*) the maximum value of the ion toroidal flow velocity obtained from same simulations as in figure 1.

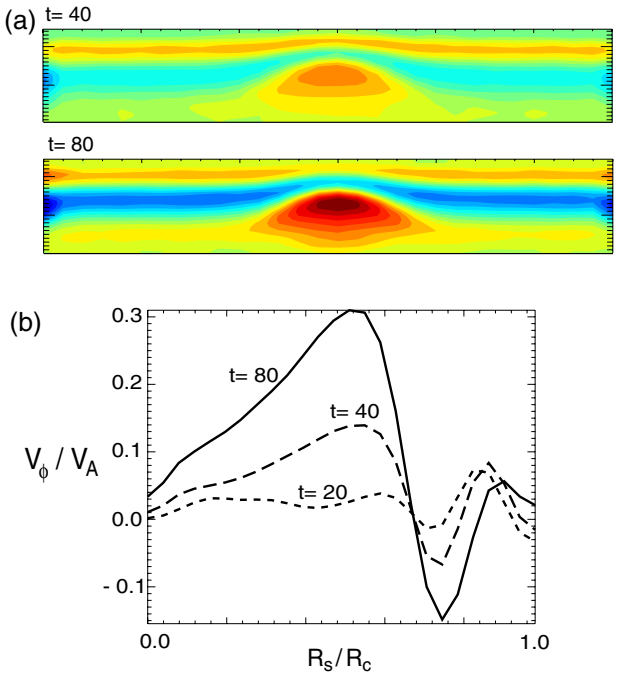

Figure 3. (*a*) Contour plots of the ion toroidal velocity in the R–Z plane at $t = 40t_A$ and $80t_A$ obtained from 2D hybrid simulations with $S^* = 20$ and $E = 4$ and (*b*) radial profiles of the ion toroidal flow velocity at the FRC midplane at $t = 20$, 40 and $80t_A$. The separatrix radius is $R_s/R_c \approx 0.6$.

particles have negative toroidal velocity, so that the particle loss results in a net flux of the negative momentum away from the separatrix region, and therefore there is a net positive ion rotation inside the separatrix (where the positive direction corresponds to the current direction). The ion toroidal spin-up in the simulations is found to be related to the resistive decay of the internal flux and the resulting loss of weakly-confined particles.

Figure 2(*a*) shows the time evolution of the toroidal angular momentum of all ions, $L = \int R \int v_\phi f \, \mathrm{d}^3\boldsymbol{v} \, \mathrm{d}^3\boldsymbol{x}$, and the angular momentum of the ions inside the separatrix region obtained in the simulations shown in figure 1. It can be seen that the net angular momentum is approximately conserved due to the imposed periodic boundary conditions in the z-direction. In contrast, the angular momentum of the part of the plasma confined inside the separatrix is positive and increases in time as the configuration decays. (Due to the imposed periodic boundary condition, particles which leave the closed-field-line region remain on the open field lines, so that the plasma outside the separatrix spins up in the negative direction.) The maximum value of the ion flow velocity is plotted in figure 2(*b*). The peak value of V_ϕ is about 0.2–0.3 V_A, which is comparable to the ion diamagnetic velocity for $S^* \approx 20$. In the final state, the ions carry a significant fraction of the total current. Similar values of the ion toroidal flow velocity have also been obtained in nonlinear 3D simulations [3].

Both 2D and 3D simulations with zero initial ion rotation demonstrate the formation of an approximate rigid-rotor profile inside the separatrix in about 40–60 Alfvén times, depending on the plasma resistivity. Poloidal contour plots and radial profiles of the ion toroidal flow velocity are shown in figure 3. Figure 3 shows that the ion flow velocity changes sign outside the separatrix, and that there is a significant velocity gradient close to the separatrix at the plasma edge. The $n = 2$ and $n = 3$ rotational instabilities are found to be localized in the vicinity of maximum velocity shear near the edge and have a similar structure to the external modes. The growth rates of the rotational modes are found to be larger in smaller-S^*, more kinetic configurations. The details of the ion toroidal spin-up determine the nonlinear evolution of these instabilities.

Toroidal ion spin-up has always been observed during the quasi-steady-state decay phase of FRC experiments [1]. The measured ion rotation frequency is comparable to the ion diamagnetic frequency $\alpha = \Omega_i/\Omega_{di} \sim 1$ by the time when about one-half of the plasma has been lost due to decay, and the $n = 2$ rotational instability begins to grow. In addition, recent observations in the TS-3 and TS-4 experiments [9] suggest that the ion toroidal spin-up plays an important role during the observed nonlinear stabilization of the $n = 1$ tilt mode. These observations are in good agreement with the results of 2D and 3D hybrid simulations described above and in [3].

A significant number of theoretical and experimental studies have been performed to investigate the plasma spin-up in FRCs [1]. Two major physical mechanisms which have been proposed to explain the observed ion rotation are particle loss [10] and the end-shortening of the radial electric field [1, 11]. The simulation results presented here provide good agreement with the observed ion rotation, even though the end-shortening mechanism is not included in our simulations due to the imposed periodic boundary conditions. The experimental estimates of the particle loss time and the spin-up time are also consistent with the assumption of spin-up resulting from the particle loss, at least for smaller FRC

devices [12, 13]. The conclusion of [11] that the particle loss will result in spin-up in the wrong direction when electric-field effects are taken into account is incorrect, because (1) it neglects the magnetization current of the lost ions and (2) it considers rotation of the lost ions relative to the laboratory frame, rather than their rotation relative to the bulk ion population.

The linear velocity profile ($V_\phi \sim R$) obtained in 2D simulations (figure 3) suggests that the distribution function f_i of the ions inside the separatrix evolves towards an exponential rigid-rotor distribution function, which corresponds to a shifted local Maxwellian distribution. The evolution of f_i toward a Maxwellian distribution in a model, which neglects ion–ion collisions, and in the absence of 3D instabilities may indicate that the stochasticity of the ion orbits plays a significant role in FRC relaxation. Earlier one-dimensional (1D) (neglecting axial variation) hybrid simulations of the ion toroidal spin-up have modelled the particle loss by removing the simulation particles whose gyrocentre was close to the separatrix [14]. The resulting plasma rotation was localized near the separatrix, in contrast to the nearly-rigid-rotation profiles found in the 2D simulations described earlier (figure 3). This difference in the rotation profiles can be explained by the complexity of the ion orbits in the 2D poloidal field and (perhaps) the model chosen for the particle loss in [14].

3. Counter-helicity spheromak merging simulations

FRC formation by the counter-helicity spheromak merging method has been developed in the TS-3 experiments in Japan [7, 9]. These experiments have shown that an FRC is formed after the opposing toroidal magnetic fields of two merging spheromaks are annihilated, and the plasma is heated to form an FRC-like pressure profile. This method allows the slow formation of an FRC with large poloidal flux, as well as studies of magnetic reconnection and MHD relaxation in high-beta plasmas [15, 16]. Theoretical studies of spheromak merging, plasma relaxation and self-organization are described in [17–24].

The SSX–FRC experiment is designed to study the new FRC formation method using counter-helicity spheromak merging and the FRC stability properties for large values of S^*. In addition, the effects of the residual (axially-antisymmetric) toroidal field on macroscopic stability properties are being studied. Experimental results demonstrate the formation of a large-beta (FRC-like) configuration with $S^* > 35$, and indicate the presence of the global $n = 1$ instability, consistent with the tilt-mode instability [8]. However, the observed growth rate of this instability is smaller by a factor of 6–8 than that of the ideal MHD growth rate. In addition, the experimental formation studies consistently show the presence of an axially-antisymmetric toroidal field, which does not completely annihilate during the reconnection. The finite toroidal magnetic field distinguishes the SSX configuration from the conventional, zero-toroidal field, FRCs. The underlying reasons for this are not yet understood. Numerical simulations using the HYM code have been performed to investigate these issues and to study 3D spheromak merging for experimentally-relevant parameters.

Two-dimensional and three-dimensional MHD simulations of counter-helicity spheromak merging have been performed for the SSX–FRC geometry and parameter range. The simulations have been performed using the 3D nonlinear resistive MHD version of the HYM code [5] with high resolution up to 127×513 grid points in the poloidal (R, Z) plane. The boundary conditions are taken to correspond to a cylindrical flux conserver which is perfectly conducting on the perturbation (fast) time-scale, but allowing for equilibrium poloidal magnetic field penetration, thus taking into account the field-line-tying effects present in the experiment. The initial spheromak formation by plasma guns has not been simulated. Instead, the initial conditions for the numerical studies have been chosen to correspond to the experimental conditions at the beginning of the spheromak merging process. Thus the initial conditions in the simulations correspond to two, low-beta, nearly force-free spheromaks with opposite toroidal magnetic fields, placed close to the device midplane.

The SSX–FRC experimental parameters are as follows: flux conserver radius and length are $R_c = 20\,\text{cm}$ and $L = 60\,\text{cm}$, respectively, the edge magnetic field is $B_0 = 1\,\text{kG}$, the plasma density is $n_0 = 10^{15}\,\text{cm}^{-3}$, the plasma temperature (after the FRC formation) is $T \approx 30\,\text{eV}$ and the FRC kinetic parameter is $S^* = R_c/\lambda_i = 28$. The Alfvén time is defined as $t_A = R_c/V_A$, which can be estimated as $t_A = 2.8\,\mu\text{s}$, where the characteristic Alfvén velocity is defined using B_0 and n_0. It has been observed that the poloidal flux at the midplane rises to its maximum value in $t \sim 10$–$15t_A$ (after the spheromaks are ejected at $t = 20\,\mu\text{s}$), and that a high-beta FRC-like configuration is formed at the midplane at $t \gtrsim 20$–$25t_A$. Growth of the $n = 1$ instability is seen at $t \gtrsim 18t_A$, when the perturbation amplitude becomes larger than the level of the $n = 1$ turbulence, i.e. at about 10% of poloidal magnetic energy density. The characteristic growth time of the $n = 1$ mode is estimated to be 10–$14t_A$, and the $n = 1$ component of the magnetic field energy becomes the dominant component at $t \gtrsim 30t_A$. The experimental parameters and results are described in greater detail elsewhere [8].

3.1. Axisymmetric simulations

A set of axisymmetric simulations of counter-helicity spheromak merging has been performed in order to study the dependence of the reconnection rate and the toroidal field annihilation on values of the plasma resistivity and viscosity. For simplicity, the resistivity and viscosity profiles have been assumed to be uniform in the simulations. The Lindquist number $S = V_A R_c/\eta$ based on classical resistivity can be estimated as $S \approx 10^3$ for $T_e \sim T_i \approx 12\,\text{eV}$. For these temperatures, the ions are collisional with $\omega_{ci}\tau_i \sim 1$, and there are several estimates for the normalized plasma viscosity coefficient $\nu = 1/Re$, where Re is the Reynolds number. The estimates of Braginskii's unmagnetized and weakly-magnetized ion viscosity are $\nu_0 \approx 8 \times 10^{-3}$ and $\nu_1 \approx 2 \times 10^{-3}$, respectively, and the gyroviscosity is $\nu_{gyro} \approx 5 \times 10^{-3}$. Due to the strong dependence on the ion temperature, there is a large uncertainty in the above values. Nevertheless, it can be seen that the SSX–FRC plasma is in the viscosity-dominated regime with $\nu > \eta$.

Numerical simulations for $\eta = 10^{-3}$ and $\mu = 10^{-3}$–4×10^{-3} show formation of an FRC in about 20–30 Alfvén times,

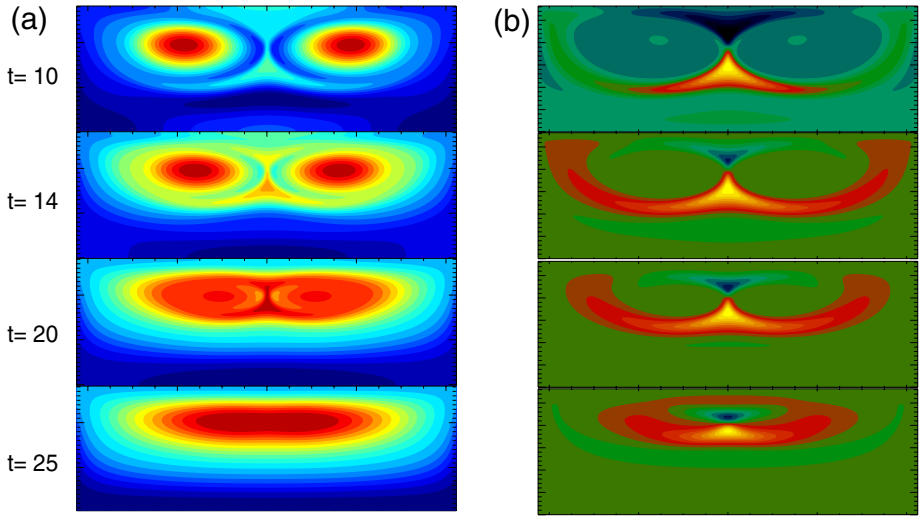

Figure 4. Contour plots of (*a*) the pressure and (*b*) the toroidal velocity at $t/t_A = 10, 14, 20, 25$ obtained from 2D MHD simulations of counter-helicity spheromak merging for $\mu = \eta = 0.001$. The velocity is normalized to the characteristic Alfvén velocity; the contour values correspond to $V_{max} = 0.4$ and $V_{min} = -0.2$ for $t = 10$–20, and $V_{max} = 0.2$ and $V_{min} = -0.1$ for $t = 25$.

where $\mu = \hat{n}\nu$ is the dynamic viscosity and $\hat{n}$ is the normalized plasma density. Evidently, large toroidal and poloidal flows with flow velocity up to ~0.5–1V_A (based on the edge field) are generated during the reconnection phase (figure 4(*b*)). The plasma pressure is significantly increased by ohmic and viscous heating, and the FRC-like pressure profile is formed due to convective transport by poloidal flows (figure 4(*a*)). The flow velocity reduces by an order-of-magnitude after the FRC formation is complete. These results agree with previous numerical studies of axisymmetric spheromak merging [17–19].

Figure 5 shows the results of five MHD simulation runs performed for values of $\eta = 2.5 \times 10^{-4}$–$4 \times 10^{-3}$ and $\mu = 10^{-3}$. It can be seen that the time for a complete reconnection depends weakly on the resistivity (this time can be approximately determined by the strong reduction in the kinetic energy in figure 5(*a*)). Thus the reconnection is complete and the FRC forms in about $20\,t_A$ for larger values of η and in about 25–$30\,t_A$ for smaller η. This is consistent with previous theoretical studies of driven magnetic reconnection [17, 18, 20]. On the other hand, the details of the time evolution of the plasma kinetic energy (figure 5(*a*)) and magnetic energy (figure 5(*b*)) vary strongly with η. For larger values of η, the kinetic energy peaks at $t \sim 5t_A$, and the flow velocity (mostly toroidal) increases with η. This initial increase in the kinetic energy is caused by the force imbalance present in the initial conditions. For values $\eta \geqslant 0.004$, the configuration decays faster than the FRC forms. In the smaller resistivity cases ($\eta \leqslant 0.002$), there is a maximum in the flow energy which occurs at $t \sim 20$–$25t_A$. This peak in the kinetic energy correlates with the large reconnection rate and the fast reduction in the magnetic energy seen in figure 5(*b*). The toroidal flow velocity in these cases is comparable to the characteristic Alfvén velocity, $V_\phi \sim V_A$.

Figure 6 shows the results of a set of MHD simulation runs performed to investigate effects of plasma viscosity for $\eta = 5 \times 10^{-4}$. The simulations have shown that the reconnection rate (as determined, for example, by the magnitude of the electric field at the reconnection X-point) is very sensitive to the value of ion viscosity, and it reduces significantly as value of μ is increased. As expected, a larger viscosity results in a strong reduction of the plasma flow (figure 6(*a*)).

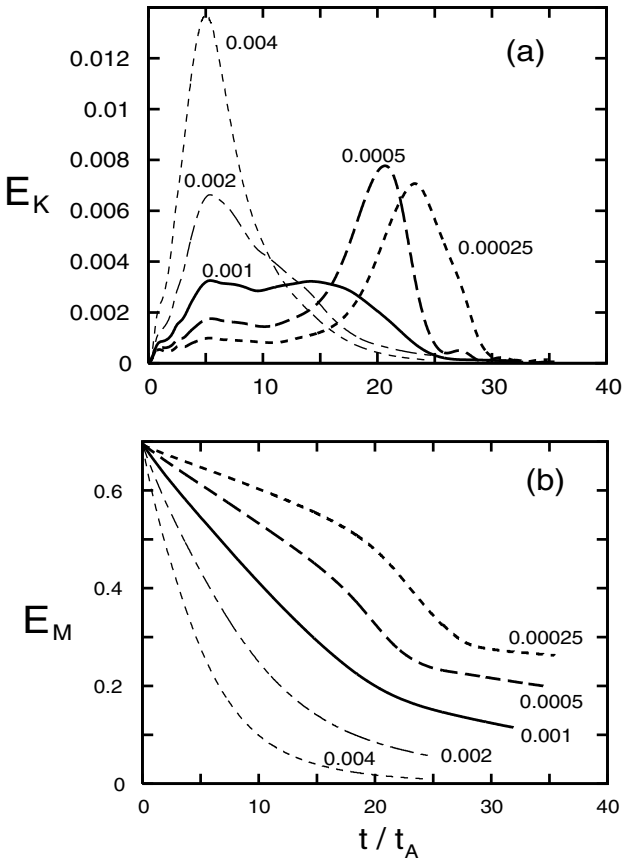

Figure 5. Time evolution of (*a*) the normalized kinetic energy and (*b*) the magnetic energy obtained from 2D MHD simulations of counter-helicity spheromak merging for $\mu = 0.001$ and several values of resistivity.

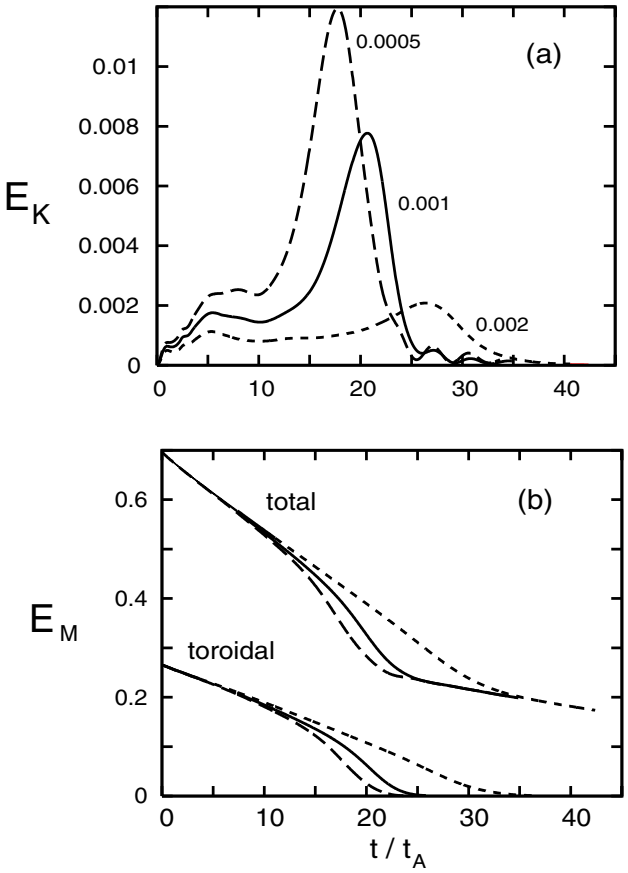

Figure 6. Time evolution of (*a*) the normalized kinetic energy and (*b*) the magnetic energy (total and toroidal) obtained from 2D MHD simulations for $\eta = 5 \times 10^{-4}$ and different values of viscosity: $\mu = 0.0005$ (- - - -), $\mu = 0.001$ (——) and $\mu = 0.002$ (– – –).

The reduced flow velocity, on the other hand, is related to a slower evolution of the toroidal field (figure 6(*b*)). Figure 7 shows contour plots of the toroidal field from the simulations with $\eta = 0.001$ and different values of viscosity $\mu = 0.001$ (low-viscosity plasma) and $\mu = 0.004$ (SSX-like plasma). It can be seen that larger values of plasma viscosity result in significant residual toroidal fields present at $t \sim 20$–$30 t_A$. Figure 7 also shows the reversal of the initial toroidal field on the outer flux surfaces at $t \gtrsim 20 t_A$ associated with the so-called 'sling-shot effect' [15, 16]. For the case with $\eta = \mu = 0.001$ (figure 7(*a*)), the magnitude of the reversed field is about 10% of the maximum toroidal field at $t = 25 t_A$. This effect is weak in the large viscosity case (figure 7(*b*)) due to the reduction in the toroidal flow velocity. Magnetic measurements in the SSX–FRC experiment do not show significant toroidal field reversal (sling-shot effect), unlike in the TS-3 and TS-4 experiments, and these observations agree with our simulation results (figure 7(*b*)). The weak toroidal field reversal in the experiment is explained by the relatively large ion viscosity in the SSX–FRC. The width of the reconnection layer estimated from the axial profile of J_R is $\delta \approx 0.8$ cm for the low-viscosity case with $\mu = 0.001$, but it increases to $\delta \approx 1.6$ cm for $\mu = 0.004$. For comparison, the experimentally measured reconnection layer is about 2–3 cm wide [25].

Therefore, the numerical results indicate that the relatively large values of plasma viscosity in the experiments ($\mu \gtrsim 0.002$) may be responsible for the finite toroidal magnetic field which is observed in SSX–FRC. The simulations predict a reduced 'sling-shot' effect in the SSX–FRC experiment and a reconnection layer width of about 2 cm, which is comparable to the experimentally measured one.

3.2. Three-dimensional simulations

Three-dimensional MHD simulations have been performed to study the 3D spheromak merging and the effects of plasma viscosity, self-generated flows and magnetic field-line-tying on the unstable global modes in the merging plasmas. Initial and boundary conditions in these simulations are identical to those in 2D simulations described in section 3.1. In addition, a random initial perturbation is applied at $t = 0$. The $n = 1$ tilt mode is found to be a dominant mode in all cases, and the configuration is tilted at the end of the simulations. Figure 8(*a*) shows the time evolution of the $n = 1$ mode obtained in four simulation runs with $\eta = 10^{-3}$ and $\mu = 5 \times 10^{-4}$–4×10^{-3}. In the linear phase, $t \lesssim 20 t_A$, the growth rate is largest for small viscosity, and the growth rate reduces as μ increases. The simulations demonstrate that large values of viscosity have a stabilizing effect on the $n = 1$ tilt mode, as well as the higher-n MHD modes. The nonlinear slow-down of the tilt instability, seen at $t \approx 20$–$25 t_A$ in low-viscosity runs, occurs when the amplitude of the $n = 1$ mode becomes comparable to that of the $n = 0$ mode. The slowing-down of the tilt motion in other cases ($\mu = 0.002$ and $\mu = 0.004$) observed at $t > 20 t_A$ is due to the evolution of the background quasi-equilibrium (from two spheromaks at $t = 0$ into FRC-like configuration) and the resistive decay of the magnetic field, which reduces the instability drive.

Figure 8(*b*) shows the time evolution of the total kinetic energy obtained for the same set of simulations as shown in figure 8(*a*). The growth of the $n = 1$ tilt mode is not seen until $t > 20 t_A$, when the amplitude of this mode becomes comparable to the $n = 0$ component of the kinetic energy. Note that by that time the growth rate of the $n = 1$ mode is reduced compared with its linear value. The calculated growth rates obtained from the simulation shown in figure 8(*a*) for $\mu = 0.004$ are $\gamma \approx 0.33\, V_A/R_s$ for $t < 20 t_A$ and $\gamma \lesssim 0.15\, V_A/R_s$ for $t > 20 t_A$. For comparison, an estimate for the ideal MHD growth rate is $\gamma_0 \sim (0.7$–$1.3) V_A/R_s$. Several factors may contribute to the reduction of the instability growth at later times ($t \gtrsim 20 t_A$), including nonlinear mode interactions and an increase of the separatrix elongation.

Additional time-evolution plots are shown in figure 9 where the peak values of the poloidal and toroidal fields, the radial current density, the axial flow velocity and the toroidal flow velocity are shown for 3D simulations with $\eta = 0.001$ and (*a*) $\mu = 0.001$ (low-viscosity plasma) and (*b*) $\mu = 0.004$ (SSX-like plasma). The initial phase of 3D simulations, shown in figures 8 and 9 ($t < 15$–$20 t_A$), is very similar to that in the axisymmetric simulations described in the previous section. However, the growth of the tilt instability can be seen in figure 9 plots at $t > 25 t_A$ for $\mu = 0.001$ and at $t > 35 t_A$ for the $\mu = 0.004$ simulation. The toroidal magnetic field reconnection rate is proportional to the radial current J_R, which

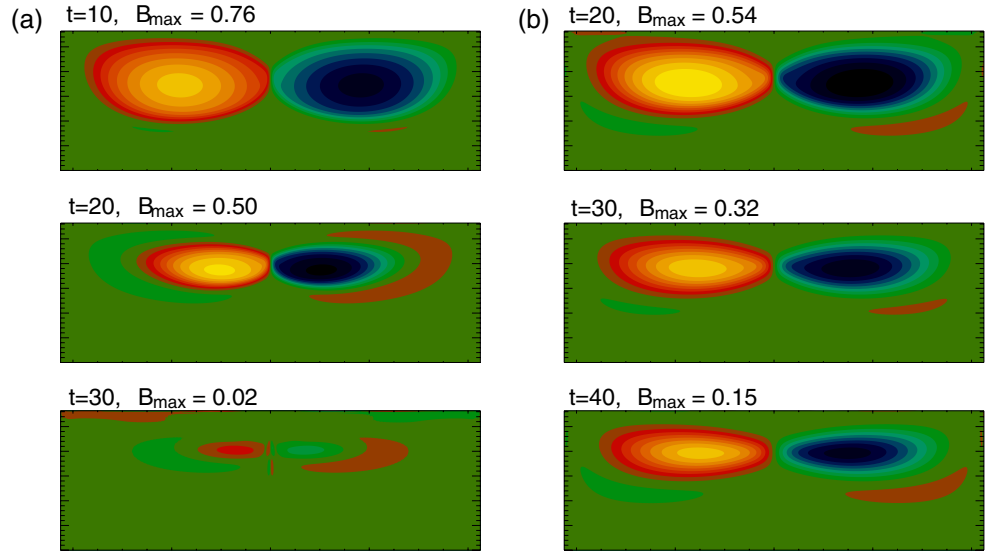

Figure 7. Contour plots of the toroidal magnetic field at the poloidal plane obtained from 2D MHD simulations with $\eta = 0.001$ and (*a*) $\mu = 0.001$ ($t/t_A = 10, 20, 30$) and (*b*) $\mu = 0.004$ ($t/t_A = 20, 30, 40$). The maximum toroidal magnetic field value (normalized to the initial edge field) is shown for each plot.

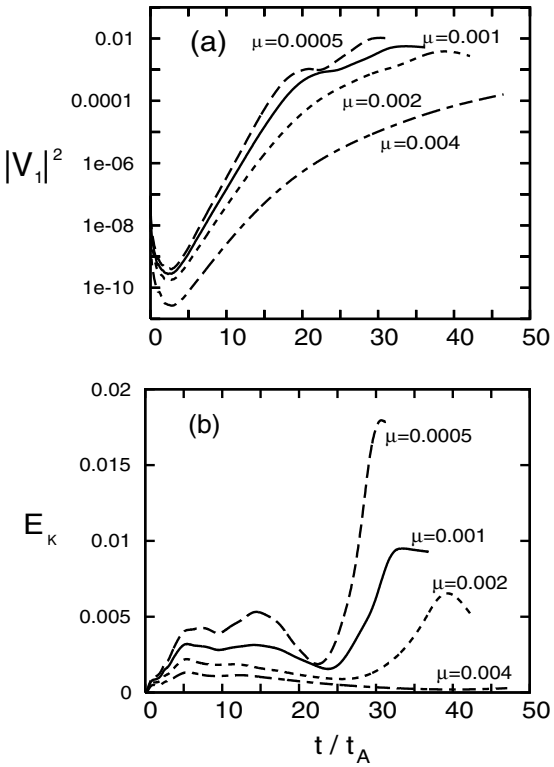

Figure 8. Time evolution of (*a*) the $n = 1$ mode energy and (*b*) the total kinetic energy obtained from four 3D MHD simulation runs of counter-helicity spheromak merging for $\mu = 5 \times 10^{-4}$–4×10^{-3}.

is significantly smaller in case (*b*) for $t \lesssim 22 t_A$. Figure 9 shows that the maximum toroidal flow velocity is reduced approximately by a factor of two when μ is increased from 0.001 to 0.004.

The possible stabilizing effect of the toroidal flows, generated during the reconnection process, appears to be less significant than the stabilizing effect of viscosity, because the growth rates for the larger V_ϕ cases (i.e. smaller μ) are larger than the growth rates for smaller V_ϕ (larger μ). The finite residual toroidal field, on the other hand, may contribute to the reduction of the growth rate of the $n = 1$ mode in the high-viscosity cases ($\mu > 10^{-3}$).

All simulations shown in this paper have been performed for realistic boundary conditions, which include the effects of magnetic field-line-tying, and which are identical in geometry and frozen-in flux with the SSX experiments. Another set of simulations (not shown) have been performed with different boundary conditions, i.e. by neglecting line-tying effects. A comparison between the runs with different boundary conditions show that line-tying effects increase the reconnection time by 5–10 t_A and reduce the $n = 1$ mode growth rate. It has also been found that the peak toroidal flow velocity is reduced by a factor of two due to line-tying effects.

In summary, the simulations show that both the large plasma viscosity and the field-line-tying boundary conditions reduce the growth rate of the tilt mode. In addition, there is a nonlinear reduction of the instability drive at the time when the mode amplitude becomes experimentally observable. These results may provide an explanation for the experimentally-measured growth rates that are about 6–8 times smaller than the ideal MHD growth rate. The SSX–FRC plasma dynamic is modified by the large viscosity due to low plasma temperature and high density in the experiment. For high-S^*, reactor-size and high-temperature FRCs, viscosity effects will not be important; on the other hand, both the line-tying effects and the effects of finite toroidal magnetic field scale to the reactor-size configurations.

4. Conclusions

The hybrid simulations presented here show that, while ion FLR effects determine the linear stability properties of

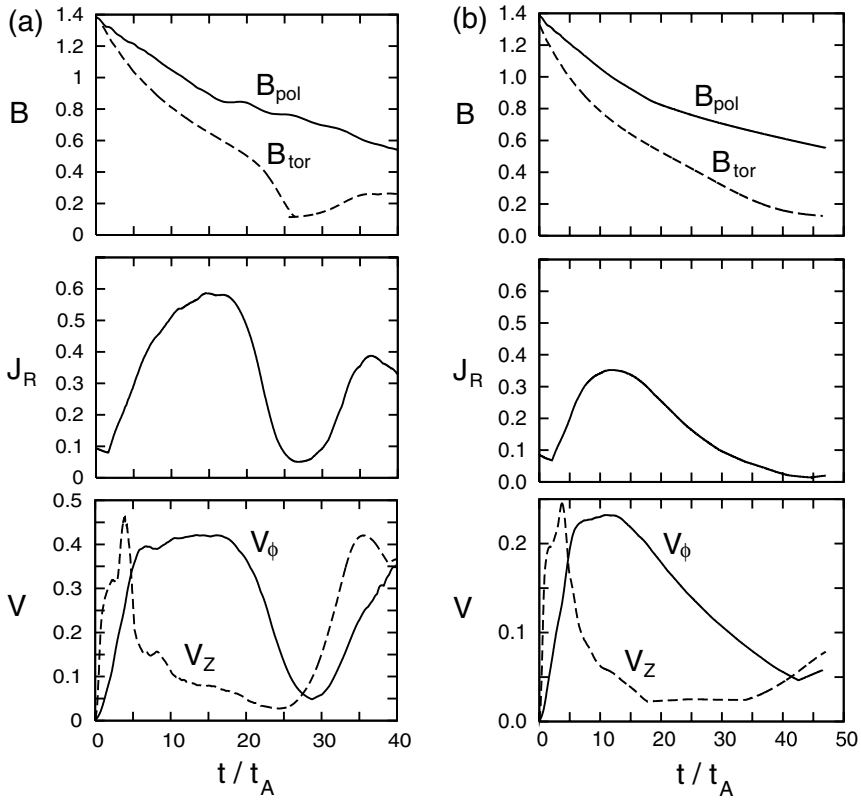

Figure 9. Time evolution of the maximum values of the poloidal and toroidal magnetic fields, the radial current density, the axial flow velocity and the toroidal flow velocity obtained in 3D simulations with $\eta = 0.001$ and (*a*) $\mu = 0.001$ and (*b*) $\mu = 0.004$.

non-rotating FRCs, the inclusion of nonlinear and ion-toroidal-flow effects is necessary for a satisfactory description of plasma behaviour in low-S^* FRC experiments. In particular, it has been shown that the ion toroidal spin-up plays an important role in FRC nonlinear evolution, including that of the $n = 1$ tilt mode.

The 3D hybrid simulations have been able to reproduce all major experimentally observed stability properties of kinetic (theta-pinch-formed) FRCs. Namely, the scaling of the linear growth rate of the $n = 1$ tilt instability with S^*/E parameter has been demonstrated for a class of elongated elliptic FRCs [3]; and ion toroidal spin-up, the nonlinear saturation of the tilt mode and the growth of the $n = 2$ rotational mode have been demonstrated. It has been shown that the loss of ions with a preferential sign of toroidal velocity due to the resistive decay of the poloidal flux results in the ion toroidal spin-up, which reproduces very well the experimentally-observed ion rotation. The time scale of the ion spin-up is determined by the flux decay time.

The MHD version of the HYM code has also been used to study FRC formation by the counter-helicity spheromak merging in support of the SSX–FRC experiment [8] and contributed to the interpretation of several puzzling experimental observations. A parameter scan, which is not easily accessible experimentally, has been carried out using numerical simulations, and it has provided a better qualitative understanding of several of the experimental results. In particular, the persistence of the residual toroidal field and the slower-than-MHD growth of the tilt instability have been shown to be related to the large plasma viscosity and line-tying effects in the SSX–FRC experiments.

Acknowledgments

This research was supported by DOE contract DE-AC02-76CH03073. The calculations were performed at the U.S. National Energy Research Supercomputing Center.

References

[1] Tuszewski M. 1988 *Nucl. Fusion* **28** 2033
[2] Ishida A., Momota H. and Steinhauer L.C. 1988 *Phys. Fluids* **31** 3024
[3] Belova E.V., Davidson R.C., Ji H. and Yamada M. 2004 *Phys. Plasmas* **11** 2523
[4] Barnes D.C. 2002 *Phys. Plasmas* **9** 560
[5] Belova E.V. *et al* 2000 *Phys. Plasmas* **7** 4996
[6] Ohtani H., Horiuchi R. and Sato T. 2003 *Phys. Plasmas* **10** 145
[7] Ono Y. *et al* 1997 *Phys. Plasmas* **4** 1953
[8] Cothran C.D. *et al* 2003 *Phys. Plasmas* **10** 1748
[9] Ono Y. *et al* 2003 *Nucl. Fusion* **43** 649
[10] Eberhagen A. and Grossmann W. 1971 *Z. Phys.* **248** 139
[11] Steinhauer L.C. 2002 *Phys. Plasmas* **9** 3851
[12] Tuszewski M. *et al* 1982 *Phys. Fluids* **25** 1696
[13] Tuszewski M. *et al* 1988 *Phys. Fluids* **31** 946
[14] Harned D.S. and Hewett D.W. 1984 *Nucl. Fusion* **24** 201
[15] Yamada M. *et al* 1990 *Phys. Rev. Lett.* **65** 721
[16] Ono Y. *et al* 1996 *Phys. Rev. Lett.* **76** 3328
[17] Watanabe T.-H., Sato T. and Hayashi T. 1997 *Phys. Plasmas* **4** 1297

[18] Sato T., Oda Y. and Otsuka S. 1983 *Phys. Fluids* **26** 3602
[19] Lukin V.S. *et al* 2001 *Phys. Plasmas* **8** 1600
[20] Biskamp D. and Welter H. 1980 *Phys. Rev. Lett.* **44** 1069
[21] Steinhauer L.C. and Ishida A. 1998 *Phys. Plasmas* **5** 2609
[22] Hameiri E. and Hammer J.H. 1982 *Phys. Fluids* **25** 1857
[23] Bhattacharyya R., Janaki M.S. and Dasgupta B. 2001 *Phys. Lett.* A **291** 291
[24] Wang Z. and Tang X.Z. 2004 *Phys. Plasmas* **11** 3502
[25] Kornack T.W., Sollins P.K. and Brown M.R. 1998 *Phys. Rev.* E **58** R36